Physica D 54 (1991) 5–19
North-Holland

PHYSICA D

Globally coupled circle maps

Kunihiko Kaneko

Department of Pure and Applied Sciences, College of Arts and Sciences, University of Tokyo, Komaba, Meguro-ku, Tokyo 153, Japan

Received 18 March 1991
Revised manuscript received 20 June 1991
Accepted 30 June 1991
Communicated by A.V. Holden

A network of circle maps is investigated. Successive transitions are found among coherent, ordered, partially ordered (PO), and turbulent phases. In the ordered phase, two-cluster attractors with similarity have a large basin volume, which are reduced to a unique circle map through a scaling transformation with two parameters. The PO phase is characterized by the increase of partition complexity. In the phase, chaotic itinerancy is observed, whose dynamics consists of quasistationary high-dimensional chaotic motion, low-dimensional attractor ruins, and switching among them. Dependence of the diffusion constant on the size and the nonlinearity clearly deviates from that by a random phase approximation, suggesting remaining correlation among elements, even in the turbulent phase.

1. Introduction

A network of chaotic elements has been investigated as a novel class for nonlinear dynamical systems with many degrees of freedom. Here we study a "globally coupled circle map" (GCM) [1–4] as an extreme limit of a long-ranged coupling and a simple network model of chaotic elements. In particular, we take the following simple example:

$$x_{n+1}(i) = x_n(i) + \frac{K}{2\pi N}\sum_{j=1}^{N}\sin\left(2\pi\left[x_n(j) - x_n(i)\right]\right), \tag{1}$$

where n is a discrete time step and i is the index of an element ($i = 1, 2, \ldots, N$ = system size).

Globally coupled maps are originally introduced as a mean-field version of coupled map lattices [5, 6], and have been studied as a novel paradigm for high-dimensional chaos [1–4]. The above model (1) has one important difference from previous GCMs. In the previous examples, an identical mean field is applied to every element. In the model (1), the coupling term can take different values by elements. Thus it is not trivial if the previously observed phenomenology in refs. [1, 2] can be applied to the above system. Another difference of our model (1) from the previous models is the existence of a conserved quantity, that is the sum of $x(i)$. Thus our dynamical system has $N - 1$ degrees of freedom. Due to this conservation, there is a Goldstone mode giving rise to the eigenvalue 1 for the Jacobian matrix.

Another motivation for the present study comes from coupled oscillators with interaction through "phases" of oscillation. There has been extensive research on coupled oscillators by Kuramoto and his coworkers, Kopell, and Ermentrout, and oth-

ers [7], inspired by the pioneering studies by Winfree [8]. Coupled circle maps in a nonchaotic regime have also been effectively used by Daido [9]. In these studies, a possible entrainment among different elements (with different native frequencies or couplings) is the focus of their interest. Our motivation is different from theirs. In our case, every element is identical, but it is able to show chaotic oscillation. Through chaos, our system can show spontaneous dynamic differentiation, termed as clusterings in ref. [1].

In neural dynamics, the importance of nonlinear dynamics has been appreciated. Even a single neuron or a small ensemble of neurons can exhibit complex dynamical behavior like chaos or a frequency locking [10]. Freeman [11] has discovered a chaotic oscillation in an olfactory bulb and discussed its significance in a searching process. Some data of EEG time series show chaotic behavior [12]. Tsuda has discovered weak chaos of a circle-map-type in his physiological neural network model [13]. He has argued various possible functions of chaos in the biological information processing.

Partial synchronization of nonlinear oscillations has been discovered in the visual cortex of a cat by Eckhorn et al. [14], and Gray and Singer [15]. Although the nature of their nonlinear oscillation has not yet been clarified, the dynamics strongly suggests the existence of chaos. Chaotic partial synchronization has been found in a partially ordered state in globally coupled maps [1]. Thus, studies of the synchronization and chaos in coupled phase models are also important for neural information processing.

A global coupling among oscillatory elements is also important in the evolution. Eigen and Schuster have introduced a model for the evolution with a global coupling through a food source [16]. A global coupling with mutation among species also leads to clusterings of oscillation of population of species [17].

An ensemble of phase oscillators with global couplings is also relevant to physics. A Josephson junction array with a coupling through an electric current is modelled by a globally coupled circle map [3, 4, 18]; that is, the use of a local map $f(x) = x + (K/2\pi)\sin(2\pi x) + \omega$ and a global coupling. Similar models can be seen in a problem of charge density wave [19]. Nonlinear optics with multi-mode excitation also provides another example of globally coupled oscillators [20].

The present paper is organized as follows. In section 2, clusterings of our attractors are studied. In particular, we show that attractors with two clusters are represented by a unique solution with two scaling parameters. All of the two-cluster attractors are similar in this sense. In section 3, phase changes of our model are shown. We have seen coherent, ordered, partially ordered, and turbulent phases successively with the increase of the coupling K. Enhancement of the fluctuation of cluster numbers is found at the partially ordered phase, analogous with the spin glass phase [21]. This variety of cluster numbers is clearly seen in the partition complexity in section 4. In section 5, chaotic itinerancy in the partially ordered phase is studied with the use of temporal change of effective degrees of freedom. The dynamics in chaotic itinerancy consists of quasistationary high-dimensional chaos and a rapid exit to one of low-dimensional "attractor ruins", and an exponential departure from it. Diffusion of an orbit through phase space is studied in section 6. A crossover from anomalous to normal diffusion is seen even in the partially ordered phase. The diffusion constant does not decrease with the increase of size to infinity, which suggests remaining correlation among elements even in the turbulent phase. Dependence of the diffusion constant on K clearly deviates from the estimate by a random phase approximation. In section 7, universality of our results is briefly mentioned with the studies of other globally coupled phase maps, where a global derivative coupling or a global average coupling is applied to local circle maps. Most of our conclusions from the map (1) are again confirmed, in addition to the discovery of degenerate torus states. Section 8 is devoted to a brief summary and future problems.

2. Clustering and coding of attractors – similarity solutions

Let us describe possible types of the attractors in our model (1). The simplest attractor is a coherent one with $x(i)=x(j)$ for all i,j. Since the force term in (1) vanishes for the coherent state, the state always implies a fixed point in time, i.e. $x(i)=\text{const.}=(1/N)\Sigma\, x(i)$. Stability of the fixed point is calculated from the Jacobian matrix $(1-K)I+(K/N)D$, where the matrix I is the diagonal matrix with elements 1 (Kronecker delta $\delta_{i,j}$), and D is the constant matrix all of whose elements are 1. Besides the unity eigenvalue, the Jacobian matrix has eigenvalues $1-K$ with an $(N-1)$-fold degeneracy. Thus the stability condition for the above coherent fixed point is given by $K<2$. In the present paper, we focus only on the nontrivial parameter regime $K>2$.

Besides the above single-clustered coherent attractor, we have attractors with clusterings. A cluster is defined as the set of elements in which $x(i)=x(j)$ for i,j, that is, $x(i)=x(j)$ for i,j belonging to a same cluster [1]. We can classify a state of our GCM by the number of clusters k and the number of elements for each cluster $(N_1, N_2, \ldots, N_k)$. Unless otherwise mentioned, we use a labelling of clusters such that $N_1 \geq N_2 \geq \ldots \geq N_k$.

If a system is attracted exactly to a k-cluster solution with $(N_1, N_2, \ldots, N_k)$, our system never goes out from the state with this clustering condition, since the motion for $x_n(i)$ and $x_n(j)$ at time $n>m$ are governed by exactly the same dynamics if $x_m(i)=x_m(j)$ holds ($x_n(i)=x_n(j)$ if $x_m(i)=x_m(j)$). Our attractor is therefore characterized by the clustering condition $[k,(N_1, N_2, \ldots, N_k)]$.

Once a system falls on a k-cluster attractor, our system is governed by a $(k-1)$-dimensional map, since there is one conserved quantity $\Sigma_i\, x_n(i)$. For example, the dynamics of a two-cluster attractor with the clustering (N_1, N_2) is governed by the following map:

$$X^1_{n+1}=X^1_n+\frac{n_2K}{2\pi}\sin\bigl(2\pi\bigl(X^2_n-X^1_n\bigr)\bigr), \tag{2}$$

where X^j_n denotes the value of the jth cluster at time n, and $n_2\equiv N_2/N$. Due to the conservation $n_1X^1_n+n_2X^2_n=\langle x\rangle$, the above dynamics is reduced to the following one-dimensional map:

$$X^1_{n+1}=X^1_n+\frac{n_2K}{2\pi}\sin\left(\frac{2\pi\bigl(\langle x\rangle-X^1_n\bigr)}{n_2}\right). \tag{3}$$

By the transformation $z_n\equiv(X^1_n-\langle x\rangle)/n_2$, the above dynamics is written as the circle map

$$z_{n+1}=z_n-\frac{K}{2\pi}\sin(2\pi z_n). \tag{4}$$

Note that the number of clusters is absorbed into the transformation; equation (4) is independent of two-cluster attractors. All the two-cluster states obey the same dynamics irrespective of the number of elements in the cluster. The dynamics of a two-cluster state with (N_1, N_2) is obtained by $X^1_n=z_n\times N_2/N+\langle x\rangle$. In other words, all the two-cluster solutions are obtained by a linear transformation from the dynamics of z. The dependence on the number of elements in a cluster is absorbed only into one parameter (amplitude of the oscillation). Thus we have many solutions with similarity.

The above argument does *not* imply that all the two-cluster states have the same stability. The stability of a two-cluster state should be judged from the N-dimensional Jacobi matrix, which requires further information. Numerically, the stability of a two cluster state decreases as the difference N_1-N_2 is increased until the two-cluster state is no more an attractor. If we start from an initial condition with a two-cluster state with $N_1\gg N_2$, the first cluster often splits into two, leading to an attractor with more than two clusters.

A two-cluster state exists as an attractor only within a range $N-N_{\text{thr}}<N_1<N_{\text{thr}}$. We have measured this threshold N_{thr}. Numerically it is not strongly dependent on the bifurcation parameter K. Roughly speaking, the threshold gradually decreases from 32 to 29, for $N=50$, as K is increased from 2.0 to 6.2. Basin volume for two-

cluster attractors gets smaller for $K > 4$, and vanishes for $K \geq 6.4$.

The argument (in the present section) on the similarity solutions for two-cluster attractors is valid for any model with the global coupling form $f(x_n(i) - x_n(j))$ with $f(-y) = -f(y)$. The above similarity solutions exist as long as the coupling is a two-body interaction satisfying Newton's third law of mechanics.

3. Phases and basin distribution

We have again discovered the following four phases, in agreement with the previous studies on globally coupled logistic maps [1].

(i) *Coherent phase* ($K \leq 2$): A coherent attractor (i.e. attractor with a single cluster) occupies (almost) all basin volumes.

(ii) *Ordered phase* ($2 < K < 3.9$): few-cluster attractors occupy (almost) all basin volumes. The phase boundary between coherent and ordered phases is located at $K = 2$, as is shown from stability analysis.

(iii) *Partially ordered phase* ($3.9 < K < 6.4$): coexistence of many-cluster and few-cluster attractors.

(iv) *Turbulent phase* ($K > 6.4$): all attractors have many ($\approx N$) clusters.

For the ordered phase, the average cluster number $\langle k \rangle$ is independent of N (not increasing with N). Indeed, $\langle k \rangle \approx 2$, independent of size, for $K \leq 3.8$. In the PO phase ($3.9 \leq K \leq 6.4$), $\langle k \rangle = cN$ with $c < 1$, while $c = 1$ in the turbulent phase. The scaled average cluster number c is plotted in fig. 1 as a function of nonlinearity K for $N = 25$ and 50. It is scaled by the size N, calculated from 500 sets of randomly chosen initial conditions. In the PO phase, the ratio c has large variation with K. This variation may be originated in window structures of low-dimensional maps corresponding to few-cluster attractors.

In the PO phase, cluster numbers differ to a large extent by attractors. The variance of cluster

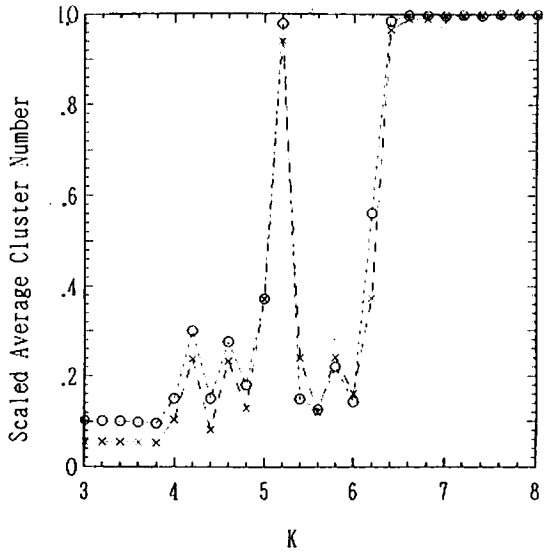

Fig. 1. Scaled average cluster number $\langle c \rangle \equiv \langle k \rangle / N$ as a function of K, with the increment of 0.2. Sizes of the system are $N = 25$ (○), and $N = 50$ (×). Numerical results in figs. 1, 2 are obtained from 500 randomly chosen initial configurations, and after discarding 40000 transients.

numbers over initial conditions is enhanced in the PO phase, as is clearly seen in fig. 2. In the ordered and turbulent phases, the variance is close to zero (or approaches zero with the increase of size N). In the PO phase, the variance seems to be roughly proportional to N, as is plotted in fig. 2, normalized by N.

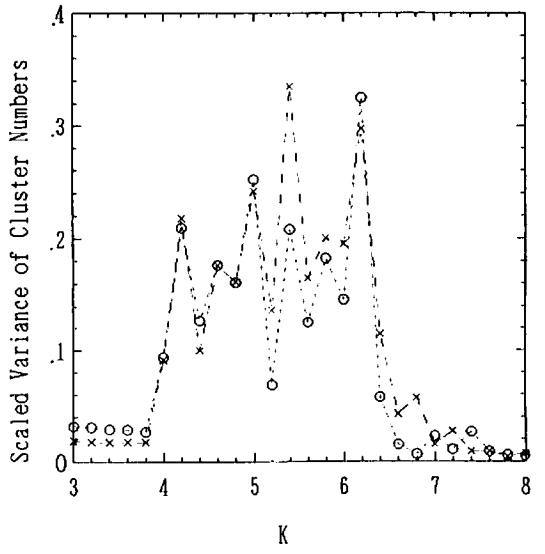

Fig. 2. Semi-log plot for the variance of the scaled cluster number $\langle (\delta c)^2 \rangle = \langle (c - \langle c \rangle)^2 \rangle$ as a function of K. Obtained from the same data as for fig. 1. $N = 25$ (○), and $N = 50$ (×).

The order-PO transition in our model is roughly associated with the onset of chaos in the circle map (4) $z' = z - (K/2\pi)\sin(2\pi z)$. This circle map shows the period-doubling bifurcation to chaos as K is increased from $K > 2$. Since the dynamics of a two-cluster attractor is represented by this circle map, the attractor shows this period doubling to chaos. The onset of chaos of the map (4) is located at $K = K_{\mathrm{dbl}} \approx 3.532\ldots$.

In the ordered phase here, almost all attractors have two clusters. Assume that our state is close to a two-cluster state. If there is no chaotic motion in the circle map (4), it is hard to imagine a mechanism to destabilize and differentiate a cluster. The ordered phase is expected to continue at least up to $K = K_{\mathrm{dbl}}$. Existence of chaos, however, is necessary but not sufficient to differentiate a cluster leading to many clusters. Indeed, the O/PO transition occurs slightly above $K = K_{\mathrm{dbl}}$ from our numerical simulation.

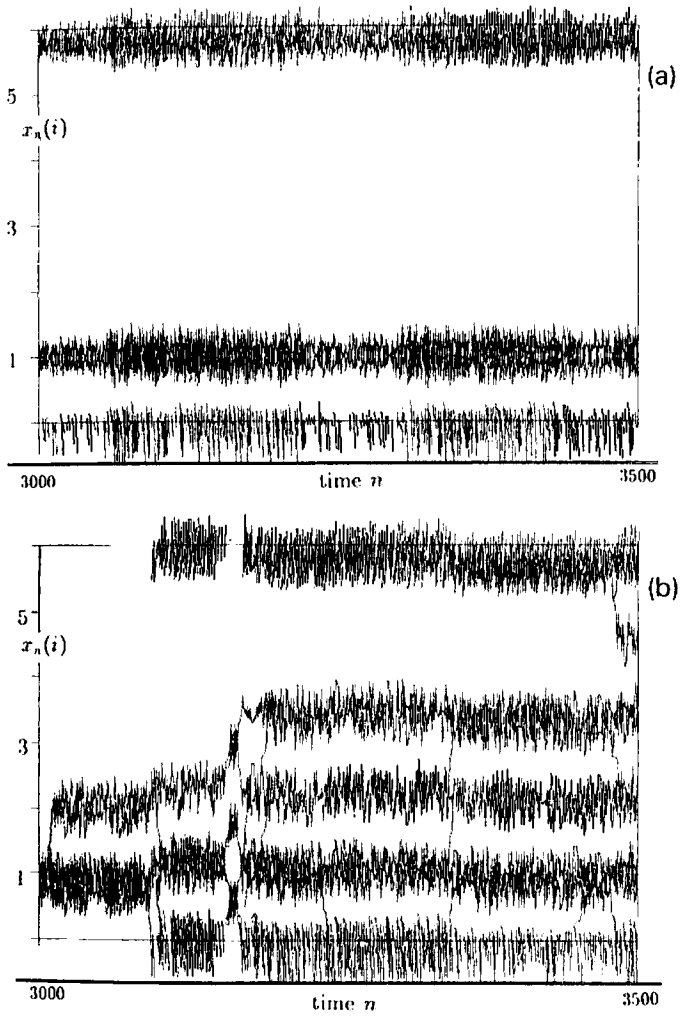

Fig. 3. Examples of timeseries of our model (1). Plotted are $x_n(i)$'s for all i, as a function of time n. They are plotted using modulus 6 ($x_n(i)$ mod 6). If there are only k lines ($k < N$), our system is fallen to a k-cluster state. $N = 40$. (a) $K = 4.4$, for time 3000–3500. The attractor has 15 clusters with the clustering (21, 4, 3, 1, 1, ..., 1). (b) $K = 4.7$, for time 3000–3500. The attractor has 17 clusters with the clustering (21, 2, 2, 2, 1, 1, ..., 1).

For $K > K^*$ ($= 4.60\ldots$) such that $\sqrt{K^{*2} - 1} - \arccos(1/K^*) = \pi$, the dynamics of the circle map (4) is not confined in a unit interval [0, 1]. The orbit starts to diffuse away to larger or smaller values triggered by its chaotic motion [22]. Thus the onset of diffusion is located exactly at $K = K^*$ for a two-cluster attractor. Although there is no rigorous proof, the onset of diffusion occurs at $K = K^*$, even for an attractor with more than two clusters, as far as we have numerically studied. In fig. 3, we have plotted the time series $x_n(i)$ with the use of modulus 6, in the PO phase. For the attractor in fig. 3b, variables $x_n(i)$ can diffuse into an arbitrary range, while the orbit in fig. 3a is localized within a box of a unit interval. Roughly speaking, the measure for a two-cluster state decreases with the further increase of K beyond K^*, although we have seen some stability windows for a two-cluster state (or a three- or four-cluster etc.). Since the single circle map (4) has windows with short periods, complicated intervention of ordered states may be rather reasonable, which is also reflected by the large variation of c in fig. 1. We have not seen any two-cluster attractor for $K > 6.3$ even if we start from a vicinity of a two-cluster state.

4. Partition complexity in the partially ordered phase

In the partially ordered (PO) phase, both few-cluster attractors and many-cluster attractors coexist. The number of clusters has no upper bound in the infinite size limit. The fluctuation of cluster

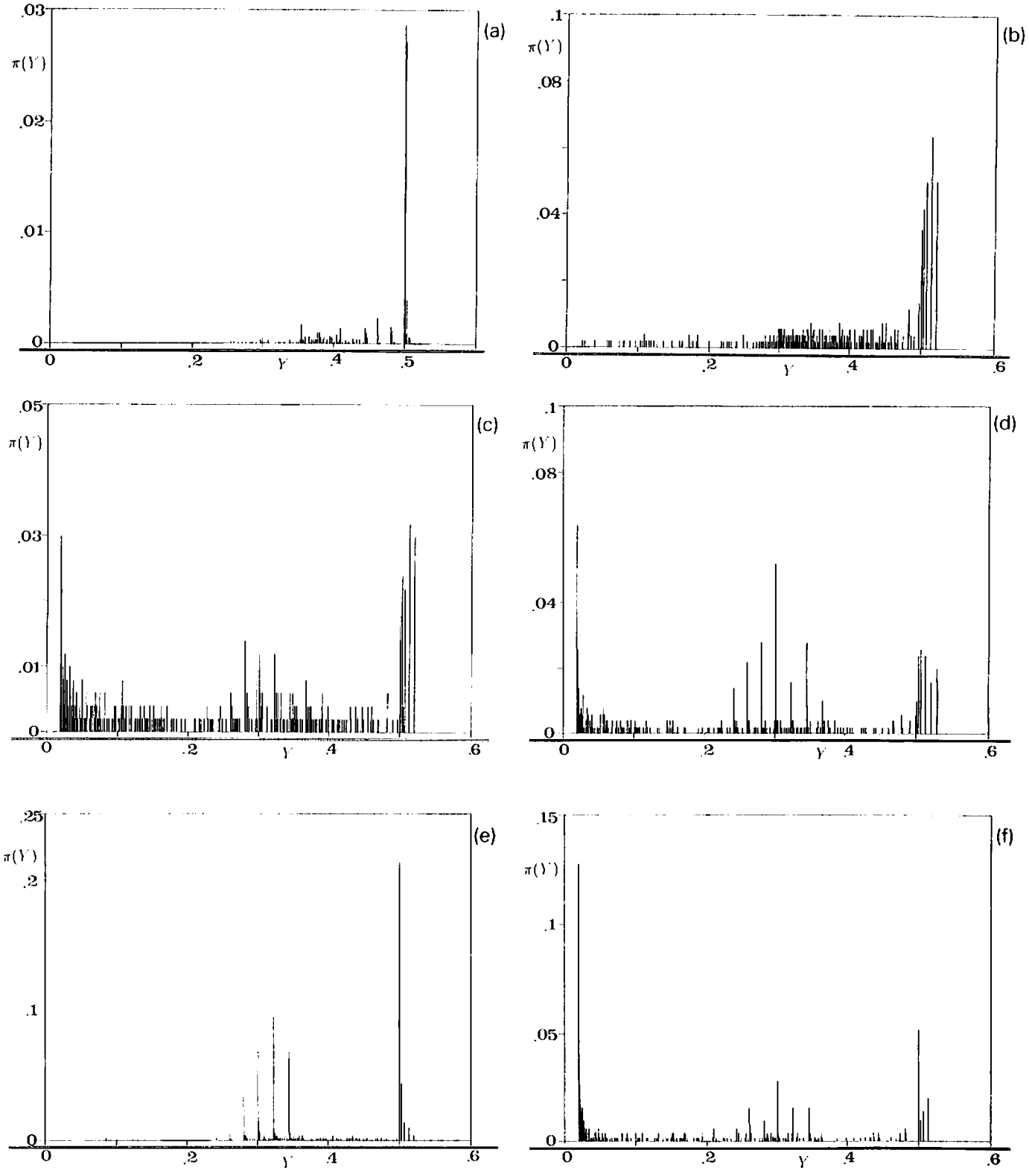

Fig. 4. Probability distribution of partitions $\pi(Y)$, calculated from 500 randomly chosen initial conditions. Y is calculated from the clustering N_i by $\sum_i (N_i/N)^2$ after discarding 40000 initial transients. $N = 50$. (a) $K = 3.6$ (b) $K = 4.0$ (c) $K = 4.2$ (d) $K = 4.0$ (e) $K = 5.8$ (f) $K = 6.2$ (g) $K = 7.0$.

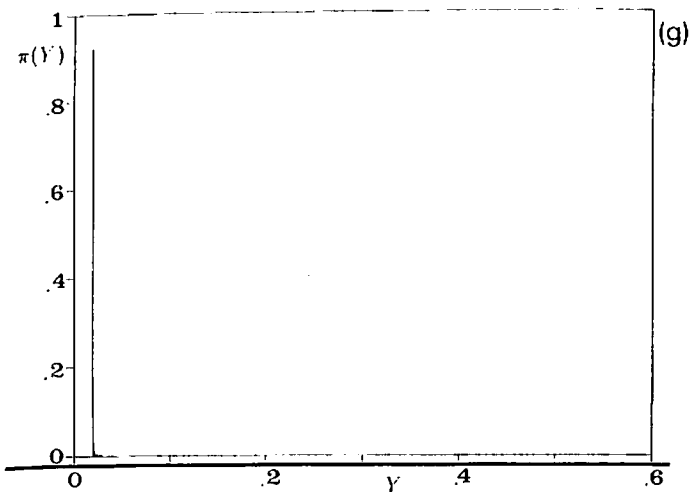

Fig. 4. (Continued.)

numbers is enhanced at the phase. We have also called this PO phase as "intermittent phase", since typical dynamics there shows an intermittent timeseries[#1].

In the PO phase, basin volume for few-cluster attractors is typically rather small. Among few-cluster attractors, there remain some measures for two-cluster attractors, although no two-cluster attractors are observed at $K \approx 4.9$. In the phase, an attractor with many clusters typically consists of a cluster with a large number of elements and many clusters with a single element.

As has been discussed [2], a feature of the partition complexity is characterized by the distribution of $Y = \sum_j (N_j/N)^2$, probability that two elements fall on the same attractor. This Y value can depend on attractors, and we can define the distribution $\pi(Y)$ sampled over initial conditions. Examples of the distribution $\pi(Y)$ are shown in fig. 4 for $K = 3.6$, 4.0, 4.2, 5.0, 5.8, 6.4, and 7.0. At the ordered phase, there is a sharp peak at the endpoint at $Y = 0.5$, corresponding to two-cluster attractors. In the PO phase Y is broadly distributed, with small peaks at the endpoints at $1/M$ $(M = 2, 3, \ldots)$, and also at $1/N \approx 0$. This clearly shows the coexistence of attractors with various partitions to clusters. The peak at $Y \approx 1/N$ grows gradually with the increase of K, till it occupies the whole probability at the turbulent phase.

[#1] In the previous paper [1], we have also another region for the partially ordered phase; glassy phase. This glassy state seems to be not an attractor but a very long transient. In our model we have again seen very long transient near the boundary between the ordered and PO phases.

5. Chaotic itinerancy at the partially ordered state

In the PO phase, chaotic itinerancy is observed for attractors with many clusters. Chaotic itinerancy (CI) is a novel universal class of dynamics in high degrees of freedom. In CI, an orbit successively itinerates over "attractor-ruins", quasistationary states with effectively low degrees of freedom. CI has independently been discovered in optical turbulence [23], model neural dynamics [24], optical information processing [25], and in globally coupled maps [1]. Experimental evidence has recently been reported in a multi-mode laser [26].

A simple way to see the temporal change in CI is the use of effective degrees of freedom, given by the number of precision-dependent clusters [1], the number of clusters within a finite precision. Instead of using the condition $x_n(i) = x_n(j)$ for the clustering, we adopt the condition $\mathrm{Int}(x_n(i) \times P) = \mathrm{Int}(x_n(j) \times P)$, with the use of the integer part $(\mathrm{Int}(z))$ of z and a large integer P to give the precision $1/P$. The precision-dependent clusters are defined with the use of this criterion for the equality.

The number of precision-dependent clusters k_n^P means the number of effective degrees of freedom, since it gives the number of variables to determine $x_{n+1}(i)$ within a given precision $1/P$, from the set $[x_n(j)]$ (at the nth step). If the number of effective degrees of freedom k_n^P is small at an instant, our motion is ordered (with low degrees of freedom) at the time. A low-dimensional ordered motion emerges from a very high-dimensional phase space.

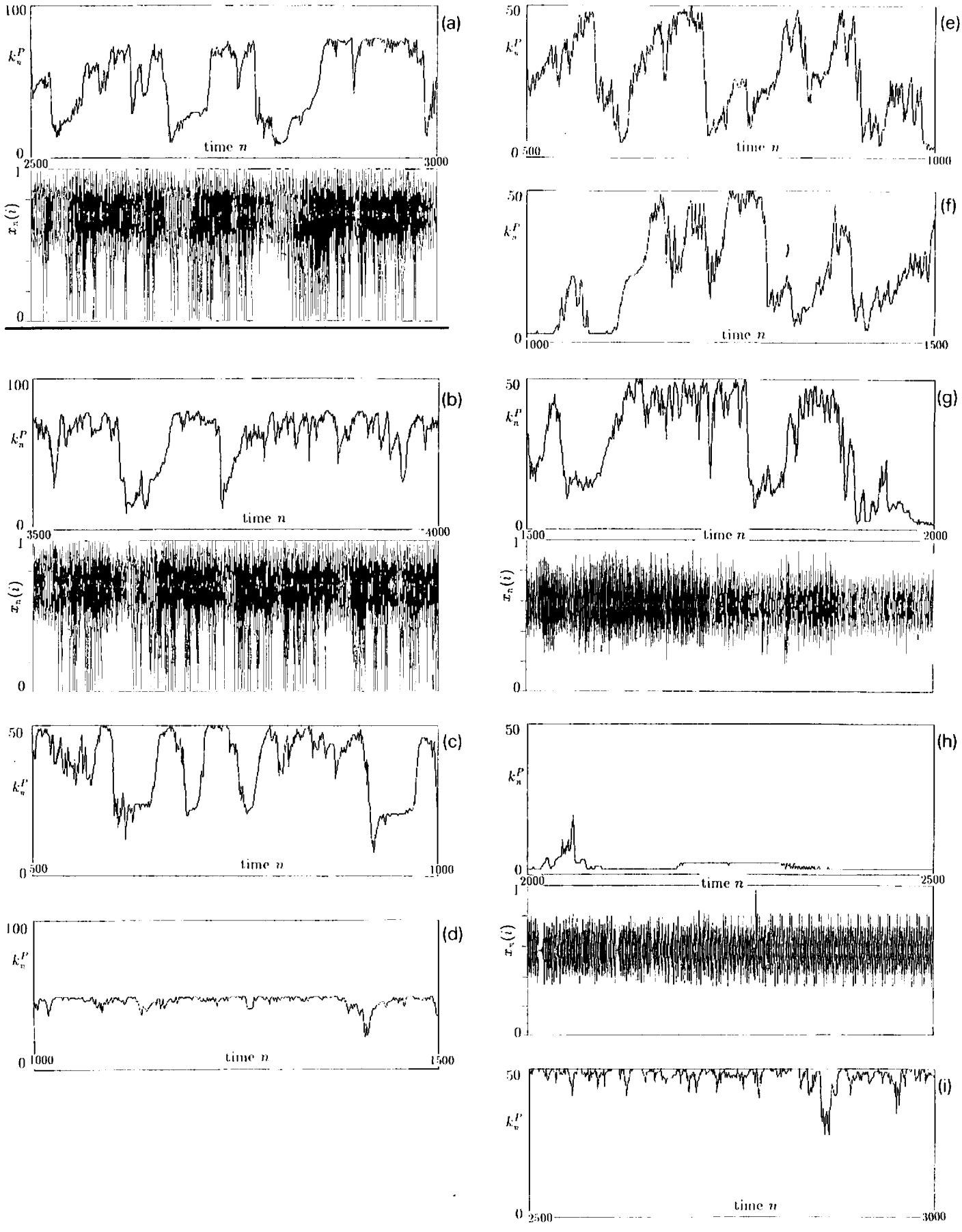
(a)
100
k_n^P
0
time n
2500
3000
1
$x_n(i)$
0
(b)
100
k_n^P
0
time n
3500
4000
1
$x_n(i)$
0
(c)
50
k_n^P
0
500
time n
1000
(d)
100
k_n^P
0
1000
time n
1500
(e)
50
k_n^P
0
500
time n
1000
(f)
50
k_n^P
0
1000
time n
1500
(g)
50
k_n^P
0
1500
time n
2000
1
$x_n(i)$
0
(h)
50
k_n^P
0
2000
time n
2500
1
$x_n(i)$
0
(i)
50
k_n^P
0
2500
time n
3000

Fig. 5. Temporal evolution of the number of precision dependent clusters. k_n^P is plotted as a function of time step n, starting with a random initial condition. $P = 10^4$.

(a) $K = 4.3$, $N = 100$ for an attractor with $k = 79$, $(12, 8, 4, 1, 1, \ldots, 1)$, for time steps from 2500 to 3000. The lower column gives the corresponding time series $x_n(i) \bmod 1$ for all i.

(b) continued from (a), for time steps from 3000 to 3500.

(c) $K = 5.0$ for an attractor with $k = N = 50$, $(1, 1, \ldots, 1)$, for time steps through 500 to 1000.

(d) $K = 5.0$, $N = 100$, for an attractor with $k = 50$, $(51, 1, \ldots, 1)$, for time steps through 1000 to 1500.

(e) $K = 4.0$, and $N = 50$, for time steps through 500 to 1000.

(f) continued from (e) for time steps through 1000 to 1500.

(g) continued from (f), for time steps through 1500 to 2000. The lower column gives the corresponding time series $x_n(i) \bmod 1$ for all i.

(h) continued from (g), for time steps through 2000 to 2500. The lower column gives the corresponding time series $x_n(i) \bmod 1$ for all i. Around the time step 2400, our systems falls on the attractor with $k = 2$, $(30, 20)$.

(i) $K = 7.5$, for an attractor with $k = N = 50$, $(1, 1, \ldots, 1)$, for time steps through 2500 to 3000.

In fig. 5, we have plotted the temporal change of the number of effective degrees of freedom k_n^P, where the precision $1/P$ is chosen to be $1/10^4$, although the following dynamical behaviors are invariant over a large range of precisions, say, from 10^{-2} to 10^{-5}. In figs. 5a–5c, sudden decreasing of k_n^P is frequently observed. After staying at low values, k_n^P starts to increase exponentially to the cluster number k. The dynamics consists of self-organization towards a lower dimensional state, residence at the state, and collapse into a high-dimensional disordered state. The following structure of CI in the phase space is suggested from fig. 5.

(1) The higher-dimensional state is quasistationary. In this higher-dimensional state, there are some "holes" connecting to a lower-dimensional state. The path from a hole is rather narrow, which directly connects the orbit to a lower-dimensional state. Indeed, the organization process to the low-dimensional state requires only few time steps. This kind of sudden escape from a quasistationary high-dimensional state to a low-dimensional one is first discovered in the supertransients in spatiotemporal chaos [27, 28], and may be a universal feature in a class of high-dimensional chaos.

(2) The organized lower-dimensional state is also quasistationary. For example, if the effective degrees of freedom are 2, our system is in the vicinity of a two-dimensional plane in the N-dimensional phase space. This two-dimensional state has both higher-dimensional stable manifolds and lower-dimensional unstable manifold(s) departing from it. The dynamics along these unstable directions leads to separation of elements belonging to a same precision-dependent cluster. This separation dynamics is formulated as chaotic revolt against the slaving principle [1]. The effective degrees increase exponentially in time, due to the chaotic instability, once an orbit enters into the path for the separation.

(3) There can be many attractor ruins. They are distinguished by the number of precision-dependent clusters k_n^P, and the partition of elements into clusters. Each attractor ruin is located in the vicinity of various k^P-dimensional spaces in the phase space. Thus the time series of effective degrees consists of (i) various plateaus at low values, (ii) exponential growth from them (iii) quasistationary fluctuation around a high value near k, and (iv) a sudden drop from it to low plateaus.

(4) Heuristically, a temporal fluctuation of effective degrees is larger as the cluster number k $(= k^\infty)$ increases. For example, an attractor with clustering $(1, 1, \ldots, 1, 1)$ has a larger variation of effective degrees than an attractor $(N/2, 1, 1, \ldots, 1, 1)$. In fig. 5d, the time series k_n^P is shown for an attractor with the clustering $[k = 39, (51, 8, 3, 2, 2, 1, 1, \ldots, 1)]$, which shows much smaller variation, compared with the other typical CI in figs. 5a–5c. A possible reason for this lies in that the organization process in fig. 5d occurs only within clusters of few elements. In an attractor with the clustering $(1, 1, \ldots, 1)$, all elements can participate in assembling to form an ordered state. On the other hand, ordering process occurs

only within clusters with $1 \sim 3$ elements, in the example in fig. 5d.

We also note that CI is also frequently observed in the transients. Even if the attractor consists of two clusters with (N_1, N_2), it may require long time steps to hit this configuration of two clusters. Before hitting this two-dimensional plane with (N_1, N_2) in the phase space, the system may approach other attractor ruins, e.g., a three-cluster state or a two-cluster state with configuration (N_1', N_2') different from (N_1, N_2) (that for the real attractor). Heuristically the transient CI has much larger and frequent variation of degrees of freedom, as is seen in figs. 5e–5h. Besides the long duration of the transients, it is almost unpredictable how and when these transients terminate.

In the turbulent phase, the effective degrees remain close to N, with a small fluctuation (see fig. 5i). Still there are rare occasions of the decrease of the effective degrees of freedom, as may be attributed to the coherent structure in the fully developed turbulence [29].

6. Diffusion

For $K > K^*$, an orbit starts to diffuse in the phase space. We have measured the following coarse-grained diffusion coefficient

$$D^i(t) = \left\langle \frac{[x_{t+t}(i) - x_t(i)]^2}{t} \right\rangle, \qquad (5)$$

where $\langle \ldots \rangle$ is the sequential temporal average (over t) [30]. For small t, $D^i(t)$ decays with some power, implying the anomalous diffusion (fig 6a). For a long time interval t, however, $D^i(t)$ approaches a constant value, meaning the normal diffusion. As far as we have checked, $D^i(t)$ always approaches a constant for large t. Even in the PO phase, the motion is diffusive, without any long-time anomalous diffusion. The crossover time from the anomalous to normal behavior is

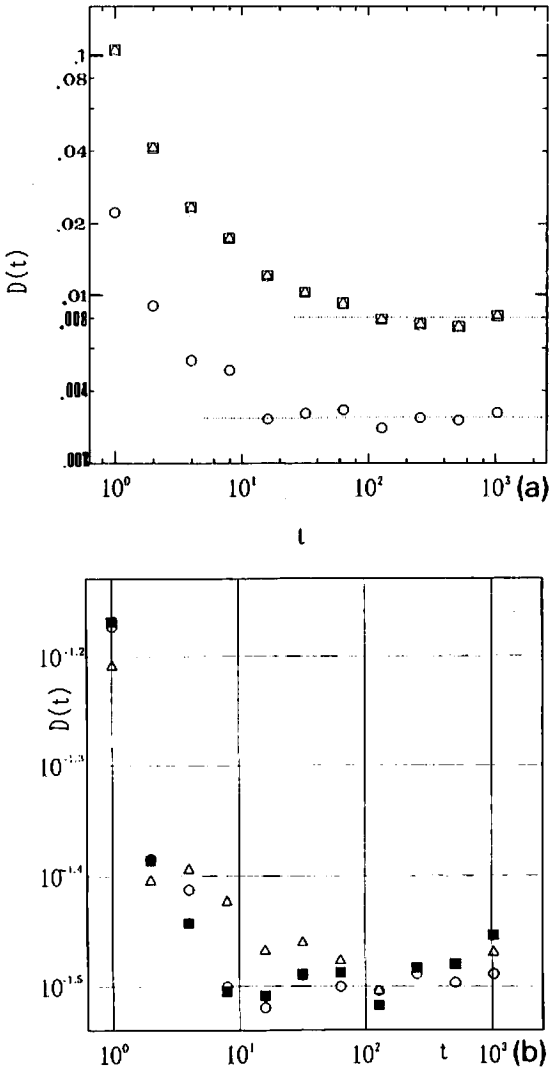

Fig. 6. Diffusion coefficient $D^i(t) = \langle [x_{t+t}(i) - x_t(i)]^2 \rangle$ as a function of coarse-grained time, where $\langle \ldots \rangle$ is the temporal average over 500 sequential temporal sets, after discarding 5000 initial time steps. $N = 20$.

(a) $K = 4.7$, for the attractor with $k = 11$, $(10, 1, 1, \ldots, 1)$. The circle ○ denotes $D^i(t)$ for the element in the first cluster (with 10 elements), while □ and △ give the data for elements for clusters with a single element. $D^i(t)$ for an element belonging to the latter 10 clusters agrees within our statistical accuracy.

(b) $K = 6.5$, for the attractor with $k = N = 20$, $(1, 1, 1, \ldots, 1)$. Three marks (○, ■ and △) give $D^i(t)$ for three different elements i. All $D^i(t)$ agree within our statistical accuracy.

quite small (less than $\mathcal{O}(10^2)$), although it can be larger in the PO phase (see fig. 6).

The diffusion constant $D^i(\infty)$ can differ among clusters. It is smaller for an element in a large cluster, as has been expected, since all other elements belonging to the same cluster does not

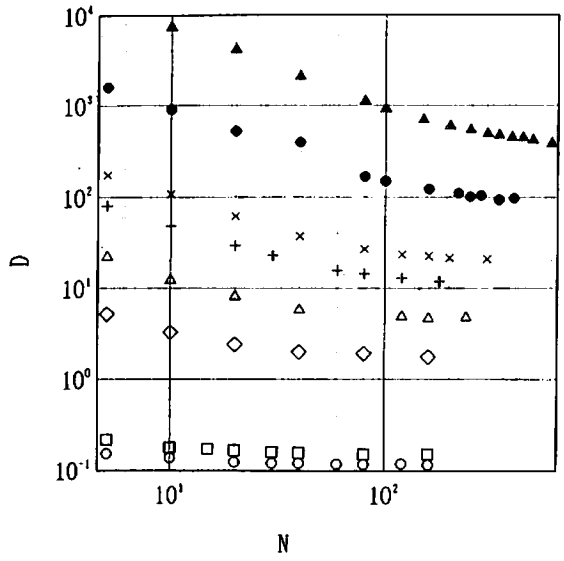

Fig. 7. Size dependence of diffusion constant. The diffusion constant $D(\infty)$ is estimated by $D(t = 100)$. $K = 8.0$ (○), $K = 10.0$ (□), $K = 50.0$ (◇), $K = 100$ (△) $K = 200$ (+), $K = 300$ (×), $K = 900$ (●), and $K = 2500$ (▲). Calculated from 100 sequential samplings, starting from a random initial condition.

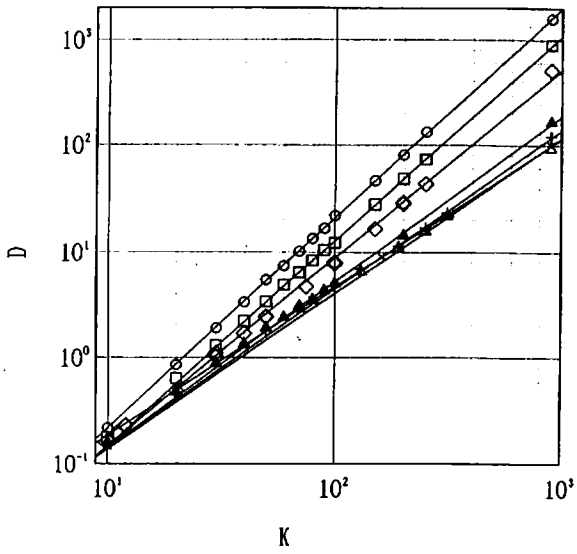

Fig. 8. Diffusion constant as a function of K. The diffusion constant $D(\infty)$ is estimated by $D(t = 100)$. $N = 5$ (○), $N = 10$ (□), $N = 20$ (◇), $N = 80$ (▲), $N = 160$ (+), $N = 250$ (×), and $N = 340$ (△). For reference, we have plotted the estimate from $D(t = 1000)$ for $N = 20$, which shows agreement within the statistical accuracy. The slopes estimated are 1.98, 1.93, 1.76, 1.55, 1.49, 1.40, and 1.45. Calculated from 100 sequential sampling, starting from a random initial condition.

apply a force on the element. In the turbulent phase, the diffusion constant is same for all elements within our statistical accuracy. There is no difference among elements.

We have measured the averaged diffusion constant $D \equiv \lim_{t\to\infty} D(t) \equiv \lim_{t\to\infty} (1/N)\Sigma_i D^i(t)$. Dependence of D on the size N is plotted in fig. 7 for various values of K. Numerically, $D(\infty)$ decreases with N up to a crossover size N_c, but then approaches a constant value for larger N, even in a turbulent attractor with N clusters. The crossover size slowly increases with K. If a random phase approximation were valid, the force term would decrease inversely proportionally to N. Fig. 7 means that the random phase approximation is not valid even if our system is strongly chaotic. The size-independent diffusion means some remaining correlation among elements, as has already been discovered in other globally coupled maps [1].

The dependence of diffusion constant on K is shown in fig. 8. Note that there is clear disagreement with the prediction $D \propto K^2$ (see fig. 8), expected from the random phase approximation, even for very large N. Indeed, the data are fit by K^α with a size-dependent exponent $\alpha \leq 2$. For a small size, the exponent agrees with 2 in consistence with the random phase approximation, but it decreases gradually with the increase of the size till it approaches 1.43 (± 0.05) for large N.

The above two observations suggest the following correlation among elements. Even if K is very large, there appears some correlation among elements. If we assume that the correlation among elements is the only source of anomalous dependence of the diffusion constant, D can be estimated by $(K/N)^2 \times \Sigma_{i,j} C(i,j)$, with $C(i,j)$ being the correlation between elements i and j. (If there is no correlation, the above form gives K^2/N as expected.) The anomalous change of diffusion with K implies the decrease of this correlation with the increase of K. The above dependence on K suggests that $C(i,j)$ $(i \neq j)$ remains finite with $N \to \infty$, which is proportional to $K^{\alpha-2}$ in the limit. We might expect some scaling form for $D(K,N)$ such as $(K^2/N) \times \bar{D}(NK^{\alpha(\infty)-2})$, with some scaling function $\bar{D}$.

However, neither this form nor some other variants fits our data well numerically so far.

We have also measured the distribution of the force term $\sin(2\pi[x_n(i)-x_n(j)])$ (for $i \neq j$), as is plotted in fig. 9. Note a sharp peak[#2] at 0, which suggests the remaining correlation even in the turbulent regime. The existence of the peak at $x(i)=x(j)$ may be one of the illustrations of the remaining correlation among elements.

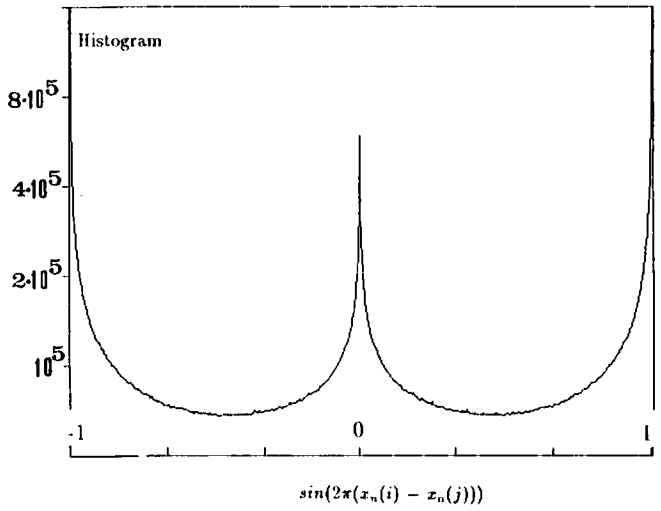

Fig. 9. Histogram for $\sin(2\pi[x_n(i)-x_n(j)])$ for $i \neq j$, sampled over all elements through 5000 to 15000 time steps. The distribution is plotted with 100 bins with the width 0.02. $K = 8.0$, $k = N = 100$.

7. Universality and partial attraction to degenerate tori

Are the existence and nature of four phases (with different clusterings) qualitatively universal among globally coupled phase models? To check the universality, we have studied the following two models:

$$x_{n+1}(i) = x_n(i) + \frac{a}{2\pi}\sin(2\pi x_n(i)) + \omega + \frac{K}{2\pi N}\sum_j \sin(2\pi[x_n(j)-x_n(i)]), \quad (6)$$

$$x_{n+1}(i) = x_n(i) + \frac{a}{2\pi}\sin(2\pi x_n(i)) + \omega + \frac{K}{2\pi N}\sum_j \sin(2\pi[x_n(j)]). \quad (7)$$

The first model (6) includes our model (1) as a special case ($a = 0$), while the latter one has been introduced by Hadley and Wiesenfeld [3] for a study of coupled Josephson junctions. These models again show the transition sequence among the coherent, ordered, partially ordered, and turbulent phases.

Examples of rough phase diagrams for the model (6) are shown in table 1. Only a coherent attractor with quasiperiodic motion exists, if a (< 1) is small enough. Around $a \approx 1$, the basin ratio for the coherent locking state starts to increase. The locking state can also lead to an attractor with few numbers of clusters, especially if the coupling K is small. As a is increased beyond 1, there appear successive changes from the ordered, partially ordered, and to turbulent phases. In the PO phase, both attractors with few and many clusters coexist. The dynamics again exhibits the typical chaotic itinerancy. As a is further increased, each circle map dynamics hits a fixed point, which is stable even in the presence of the coupling. There, the coherent fixed point attractor occupies the whole basin volume.

In model (7) we have again seen a transition sequence from ordered to PO, and to turbulent phases for $a > 1$. For a single circle map ($K = 0$), the ratio for a frequency locking state (in the parameter space ω) increases quite rapidly around $a = 1$ [6]. With the increase of locking ratio, our coupled model falls on an ordered state with few number of clusters. For example, attractors with 3 or 4 clusters occupy a large basin volume at $1.0 < a < 1.2$ (for $K = 0.1, 0.2, 0.5$). Around $1.2 < a < 1.3$, attractors with many (but

[#2] The other peaks at ± 1 are mainly due to the vanishing derivative $(\sin(2\pi(y))'$ at $y = \pm \frac{1}{2}$. The peak at 0 is not such an artifact.

Table 1
Rough phase diagram for the model (6), which is obtained from the clusterings of attractors from 100 initial conditions, with $N = 50$. Results for $K = 0.01$, 0.2 and 0.5 are given, while a is changed by 0.1. H_l stands for a coherent (homogeneous) quasiperiodic (torus) state, H_p for a coherent periodic, and H_f for a coherent fixed-point, while O_l stands for an ordered state with rich l clusters, PO for a partial ordered state, and T for a turbulent state

K	a					
	0.1	0.5	1.0	1.5	2.0	2.5
0.5	H_t H_t H_t H_t	H_t H_t H_t H_t H_t	H_p H_p H_p O_2 H_p	H_p T T T T	T H_f H_f H_f O_2	O_2
0.2	H_t H_t H_t H_t	H_t H_t H_t H_t H_t	H_p H_p H_p PO PO	PO T T T PO	H_f H_f H_f H_f H_f	H_f
0.01	H_t H_t H_t H_t	H_t H_t H_t H_t H_t	O_7 O_3 O_2 O_8 T	T T T PO T	H_f H_f H_f H_f H_f	H_f

less than N) clusters coexist, with the chaotic itinerancy. With the further increase of a, the system enters into a turbulent phase. Cluster numbers are N for almost all attractors for $1.3 \leq a \leq 1.7$ (for $K = 0.2$). Further increase of a leads our system again to the ordered phase with two clusters.

To sum up, both the models (6) and (7) belong to the same qualitative universality class with the model (1), except the following novel phase, which appears in the model (7) at $a < 1$. The phase is a quasiperiodic state with partial attraction, which is termed as "attractor crowding" by [3]. The number of clusters is N (elements are completely desynchronized). We have calculated Lyapunov spectra for this state. Lyapunov spectra, whose maximum is zero, have many ($N - 3 \sim N - 1$) degenerate null Lyapunov exponents, meaning a highly degenerate torus state.

In this degenerate state, mean-field fluctuation vanishes with the size. To see this, we have measured the temporal distribution of the mean-field $h_n \equiv (K/2\pi N)\Sigma_j \sin(2\pi[x_n(j)])$. The variance of the distribution of h_n decays roughly with $1/N$, in contrast with the variance for the turbulent phase, which does not decay with N (fig. 10b). Thus the mean-field distribution approaches a delta function in the limit of $N \to \infty$ for the degenerated torus state. The dynamics of the model (7) approaches N independent circle maps, leading to a state of degenerate independent tori. There is no attraction into a lower-dimensional phase space. The initial N-dimensional phase space is almost preserved.

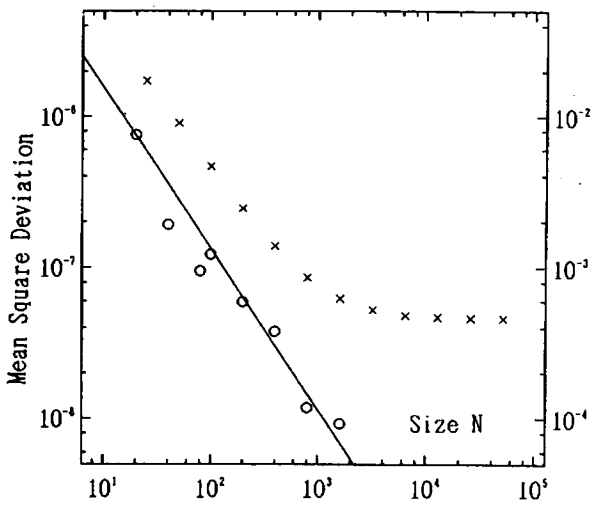

Fig. 10. Variance of the mean field $h_n = \Sigma_j \sin(2\pi x_n(j))$ for the model (7). The variance $\langle (h - \langle h \rangle)^2 \rangle$ is plotted as a function of size N, calculated from 10000 temporal steps after discarding 3000 transient steps starting from a random initial condition; $K = 0.2$, $\omega = 0.3$; O ($a = 0.5$) with the scale in the left axis, (for a degenerate torus state); × ($a = 1.5$), with the scale in the right axis (for a turbulent state). The slope of the line in the figure is -1.

As long as N is finite, there remains small correlation among elements, which leads to the existence of negative Lyapunov exponents. Roughly speaking, our dynamics can be replaced by a direct product of degenerate tori in addition to the attraction to a lower-dimensional state induced by small correlation among elements. This attraction is partial, and most of initial information is not lost, such as the ordering of $x_n(i)$ [3]. The so called "attractor" crowding is originated in this absence of attraction in the $N \to \infty$

limit, and in the partial attraction onto a highly degenerate torus[#3].

8. Summary and discussion

We have studied globally coupled phase models. Attractors are characterized by cluster numbers and the clustering distribution. Phases are defined through the basin volume for attractors with each clustering. Successive changes among the coherent, ordered, partially ordered, and turbulent phases are found. In the ordered phase, two-cluster attractors have large basin volumes. All the two-cluster attractors have similarity, and are represented by two parameters, one for the mean value and the other for the amplitude of oscillation. In the partially ordered phase, clusterings have a large variety of partition. The enhancement of the clustering variety is clarified by the fluctuation of cluster numbers and $\pi(Y)$, i.e., the distribution of the probability that two elements fall on the same cluster.

In the partially ordered phase, chaotic itinerancy is observed, as is characterized in the large temporal variation of effective degrees of freedom. Our chaotic itinerancy consists of a quasi-stationary high-dimensional state, exits to ordered states with low effective degrees of freedom, reside therein, and chaotic exits from them. Very long transients with the chaotic itinerancy are also noted. Diffusion of an orbit in the phase space shows a crossover from the normal to anomalous behavior. The diffusion constant does not decrease with size, due to a strong correlation among elements. Its K-dependence also clearly deviates from that expected by the random phase approximation.

Some other phase models are also studied, which again show the same qualitative universality. A novel state therein is a degenerate torus state with partial attraction, found in the globally coupled circle map with weak nonlinearity.

Most of our clustering results belong to the same qualitative universality class as the globally coupled logistic map. Since the mean field in the present model can take different values by elements, in contrast with the previous studies [1], this allocation to the same class is not trivial. In our model, the partially ordered phase with chaotic itinerancy is seen in much larger parameter regions than in the previous model. We do not yet know if this observation is a general feature in a model with element-dependent global coupling values.

Bifurcations to attractors with different clusterings introduce successive symmetry breakings with respect to the full permutation group S_N among all the identical oscillators. It will be important to analyze our clustering changes with the use of the bifurcation theory in systems with symmetry [31].

Relevance of coupled phase models with chaos to neural dynamics has recently been emphasized [32]. Search with chaotic itinerancy, switching among attractors, and the possibility of dynamical categorization have been discussed [1, 24]. Capability of the information processing is thought to be rather large in the partially ordered phase [1]. The predominance of the partially ordered phase in the parameter space and the clear chaotic itinerancy in our model will give promising possibilities for future studies in the biological information processing.

A Hamiltonian version of the present model has been studied by Konishi and the author [33, 34]. In the model we have again found a new type of partially ordered states, which will be reported elsewhere.

Acknowledgements

The author would like to thank T. Konishi, I. Tsuda, and K. Ikeda for useful discussions. He would also like to thank the National Institute for Fusion Study at Nagoya for the computational

[#3] In this sense the term "attractor crowding" may be misleading.

facility of FACOM M380 and VP200. This work is partially supported by Grants-in-Aid for Scientific Research from the Ministry of Education, Science, and Culture of Japan.

References

[1] K. Kaneko, Phys. Rev. Lett. 63 (1989) 219; Physica D 41 (1990) 38; Phys. Rev. Lett. 65 (1990) 1391; 66 (1991) 243 (E).
[2] K. Kaneko, J. Phys. A 24 (1991) 2107.
[3] P. Hadley and K. Wiesenfeld, Phys. Rev. Lett. 62 (1989) 1335.
[4] P. Alstrom and R.K. Ritala, Phys. Rev. A 35 (1987) 300.
[5] See, e.g., J. P. Crutchfield and K. Kaneko, in: Directions in Chaos (World Scientific, Singapore, 1987) pp. 272–353; K. Kaneko, Prog. Theor. Phys. 72 (1984) 480; 74 (1985) 1033; Physica D 23 (1986) 436; 34 (1989) 1; 37 (1989) 60 and references therein.
[6] K. Kaneko, Collapse of tori and genesis of chaos in dissipative systems, Ph.D. Thesis, 1983 (enlarged version published by World Scientific, Singapore, 1986).
[7] Y. Kuramoto, Prog. Theor. Phys. Suppl. 79 (1984) 223; G.B. Ermentrout and N. Koppel, SIAM J. Math. Anal. 15 (1984) 215; K.Y. Tsang, R.E. Nirollo, S.H. Strogatz and K. Wiesenfeld, Physica D 48 (1991) 102–112.
[8] A. Winfree, The Geometry of Biological Time (Springer, Berlin, 1980).
[9] H. Daido, Prog. Theor. Phys. 75 (1986) 1460.
[10] H. Hayashi et al., Phys. Lett. A 88 (1982) 265; K. Aihara and G. Matsumoto, in: Chaos, ed. A.V. Holden (Princeton Univ. Press, Princeton, 1986).
[11] W. Freeman and C.A. Skarda, Brain Res. Rev. 10 (1985) 147; W. Freeman, Brain Res. Rev. 11 (1986) 259.
[12] A. Babloyanz and A. Destexhe, Proc. Natl. Acad. Sci. 83 (1986) 3513.
[13] I. Tsuda, E. Koerner and H. Shimizu, Prog. Theor. Phys. 78 (1987) 51; I. Tsuda, Prog. Theor. Phys. Suppl. 79 (1984) 241.
[14] R. Eckhorn et al., Biol. Cybernetics 60 (1988) 121.
[15] C.M. Gray, P. Koenig, A.K. Engel and W. Singer, Nature 338 (1989) 334.
[16] M. Eigen and P. Schuster, The Hypercycle (Springer, 1979).
[17] K. Kaneko and T. Ikegami, preprint (1991); see also T. Ikegami and K. Kaneko, Phys. Rev. Lett. 65 (1990) 3352.
[18] S. Coppersmith, Phys. Rev. A 38 (1988) 375.
[19] H. Ito, private communication.
[20] K. Wiesenfeld et al., Phys. Rev. Lett. 65 (1990) 1749; C. Bracikowski and R. Roy, Chaos 1 (1991) 49; H.G. Winful and L. Rahman, Phys. Rev. Lett. 65 (1990) 1575.
[21] M. Mezard, G. Parisi and M.A. Virasoro eds., Spin Glass Theory and Beyond (World Scientific, Singapore, 1987).
[22] T. Geisel and J. Nierwetberg, Phys. Rev. Lett. 48 (1982) 7; S. Grossman and H. Fujisaka, Phys. Rev. A 26 (1982) 1779.
[23] K. Ikeda, K. Matsumoto, and K. Ohtsuka, Prog. Theor. Phys. Suppl. 99 (1989) 295.
[24] I. Tsuda, in: Neurocomputers and Attention: Neurobiology, synchronisation and chaos, eds. A.V. Holden and V.I. Kryukov (Manchester Univ. Press, 1991).
[25] P. Davis, ATR Res. Lab. preprint (1990).
[26] F.T. Arrechi, G. Giacomelli, P.L. Ramazza and S. Residori, Phys. Rev. Lett., in press.
[27] J.P. Crutchfield and K. Kaneko, Phys. Rev. Lett. 60 (1988) 2715.
[28] K. Kaneko, Phys. Lett. A 149 (1990) 105.
[29] See, e.g., A.K.M.F. Hussain, J. Fluid Mech. 173 (1986) 303.
[30] K. Kaneko and T. Konishi, Phys. Rev. A 40 (1989) 6130.
[31] M. Golubitsky, I. Stewart and D.G. Shaeffer, Singularities and Groups in Bifurcation Theory II (Springer, Berlin, 1988).
[32] I. Tsuda, in: World Future, in press (1991); I. Tsuda and K. Kaneko, in preparation.
[33] T. Konishi and K. Kaneko, J. Phys. A 23 (1990) 715.
[34] T. Konishi and K. Kaneko, in preparation.